Stirling RA, Glendinning S, Davie CT.

Modelling the deterioration of the near surface caused by drying induced cracking.

***Applied Clay Sciences* 2017, 146, 176-185.**

Applied Clay Science 146 (2017) 176–185

Contents lists available at ScienceDirect

Applied Clay Science

journal homepage: www.elsevier.com/locate/clay

Research paper

Modelling the deterioration of the near surface caused by drying induced cracking

Ross A. Stirling*, Stephanie Glendinning, Colin T. Davie

School of Civil Engineering and Geosciences, Newcastle University, Newcastle, UK

ARTICLE INFO

Keywords:
Desiccation
Cracking
Unsaturated soil
Tensile strength
Deterioration

ABSTRACT

Assets such as roads, railways, pipelines and flood embankments are inherently vulnerable to the action of weather and in the long term, climatic change. Their exposure makes them highly susceptible to deterioration during the course of their design life and beyond. The drivers of deterioration are believed to be human (e.g. traffic, maintenance) and environmental (e.g. weather, pollution, burrowing) but the actual deterioration *processes* are not well understood. Among the weather-driven processes, it is believed that desiccation of the near-surface and the development of cracking can significantly influence the mechanical, hydrological and thermal behaviour of geotechnical structures primarily by impacting the transmission of water between the atmosphere and soil. Enhanced infiltration during rainfall events can potentially lead to rapidly elevated pore water pressures and reduced shear strength and is widely cited as the strength reduction mechanism behind the wide spread failure of infrastructure slopes. This paper describes the development of a pseudo-discrete continuum Finite Difference model and its application to investigate the influence of soil properties (including elastic modulus, hydraulic conductivity and soil-water retention) on the desiccation process and eventual crack initiation and propagation behaviour. The generation of a desiccated crust typified by highly negative pore pressures and increasingly disintegrated texture is demonstrated. The influence of projected higher drying rates and seasonal drying-wetting cycles (that could result from climate change) on crack pattern development is investigated to gain an understanding of progressive deterioration. This points towards the potential for increased future deterioration rates of geotechnical infrastructure.

1. Introduction

Geotechnical assets are fundamental to the delivery of critical services, such as roads, railways, pipelines and flood protection structures and are characterised by a number of common features. These include a relatively long physical length and design life (with many assets actually being maintained as serviceable for long periods in excess of their design life). This spatial and temporal 'length' means that these assets are also characterised by their exposure to the action of weather, including a range of extreme events, and climatic change, which causes the asset to 'deteriorate'. These assets are all constructed either with or within engineered or natural soil, making them susceptible to weather driven changes in water content which accelerates and/or causes further 'deterioration'. Furthermore, the soil component of the asset is materially highly heterogeneous, meaning that its current state (relative to the required design performance) is unknown, as is its rate of deterioration. This means that our most critical infrastructure is in an unknown state of repair, and there is currently little understanding of the rate of deterioration of these assets and how this may be affected by extreme weather events or climate change. There is an urgent need to better understand weather-related deterioration processes, the materials most susceptible to these processes and how these might alter in a changing climate.

One such deterioration process is desiccation cracking, a widely observed phenomenon brought about by changes in volume due to drying. The majority of published studies are concerned with investigating small-scale cracking behaviour under controlled laboratory conditions and, in recent years, the development of sophisticated numerical tools to characterise this behaviour e.g. Konrad and Ayad, 1997; Yesiller et al., 2000; Albrecht and Benson, 2001; Kodikara et al., 2004; Nahlawi, 2004; Nahlawi and Kodikara, 2006; Rodriguez et al., 2007; Tang et al., 2008; Peron et al., 2009; Tang et al., 2010; Sánchez et al., 2014. Studies into cracking commonly necessitate the simulation of water removal which is primarily the result of seasonal drying due to evaporation. Additionally are the effects of vegetation and the infiltration potential of the soil surface; therefore, cracking related

* Corresponding author.
E-mail address: Ross.Stirling@ncl.ac.uk (R.A. Stirling).

http://dx.doi.org/10.1016/j.clay.2017.06.003
Received 8 March 2017; Received in revised form 16 May 2017; Accepted 4 June 2017

deterioration is largely governed by climate. The implications of climate on shrink-swelling behaviour are central to the sustainable management of our geotechnical infrastructure. It was reported by Jones and Jefferson (2012) that damage due to shrink-swell cost the UK economy £3 billion in the preceding 10 years, surpassing that of any other geo-hazard. Furthermore, an annual cost of $15 billion due to shrink-swell damage to buildings and infrastructure is estimated in the US (Jones and Jefferson, 2012). Projected climate change for the UK indicates an increased occurrence of warmer summers causing drying and a greater number of short duration and high intensity rainfall events likely to cause increased surface run-off and crack infiltration (Hulme et al., 2002; Jenkins et al., 2010), thus exacerbating the issue of climate driven deterioration.

The availability of water immediately below the drying surface is recognised to fundamentally govern the moisture exchange mechanism between the soil and atmosphere (Wilson et al., 1997; Tran et al., 2016). The high pore-water suctions generated in the very shallow zone as soil dries strongly influence the actual evaporation via soil surface resistance (Tran et al., 2016). Furthermore, suctions > 1500 kPa (known as the 'vegetation wilting point') inhibit the uptake of water by roots, thus restricting the extraction of water by transpiration. A reduced rate of total water loss during drying events limits the generation of suction at depth that is required to maintain effective stress through wetter periods (leading, for example to slope instability). Very low unsaturated hydraulic conductivity resulting from desiccation limits the migration of water from beneath and also reduces the infiltration potential during rainfall events. This leads to increased run-off which has the potential to contribute to by-pass flow via crack networks, allowing water to dissipate suctions more rapidly, thus enhancing the risk of instability.

The study presented herein makes several significant scientific advances over previous work in this field. The numerical model developed is capable of capturing the influence of soil properties (mechanical and hydrological) on the weather-driven deterioration process of cracking and further development of crack patterns with drying-wetting cycles. Furthermore, the material properties used in the simulation have been determined from both laboratory and field testing of the same soil and provide a comprehensive suite of soil-specific parameters. Additionally, field testing was used to determine the in-situ density and permeability parameters used in the study to enhance the relevance of the work to field conditions. The model developed has then been employed to investigate the cracking behaviour that results from drying in soils of differing material stiffness, permeability and soil-water retention properties as well as the effect of tensile strength reduction (i.e. the resistance of soil to cracking) due to seasonal drying-wetting cycles. The significance of this work is that the susceptibility of engineering soils to cracking related deterioration may be better understood in the context of current and future climatic conditions. This understanding can then be used to determine the implications of both extreme and repeated seasonal drying on the deterioration of geotechnical infrastructure. This has the potential to be used to quantify the increase in investment required to maintain the long-term performance of assets.

2. Material

Lower Durham Boulder Clay was simulated in this work and was used in the construction of the BIONICS full-scale trial embankment near Newcastle-upon-Tyne UK as described in Hughes et al. (2009) and Glendinning et al. (2014). The use of this material enabled both laboratory derived soil parameters and as-placed parameters to be included. The following composition was established by XRD analysis: quartz 63.5%, feldspar 7%, phyllosilicates/clay minerals including undifferentiated mica species 18.2%, kaolinite 7.1% and chlorite/smectite 0.7%. A range of Geotechnical classification tests have also been performed, the results of which are presented in Table 1.

Table 1
Material classification.

Property		Value
Liquid limit[a], L_l (%)		45
Plastic limit[a], P_l (%)		24
Plastic index[a] (%)		21
Optimum moisture content[b] (%)		15
Maximum dry density[b] (Mg/m^3)		1.82
Particle density[a] (Mg/m^3)		2.64
In situ dry density at < 1 m depth (Mg/m^3)		1.65
PSD[a]	Coefficient of uniformity, Cu	9.6
	Coefficient of curvature, Cz	1.2

[a] BS 1377-2 (British Standard Institute, 1990a) particle density determined using the Gas Jar method.
[b] BS 1377-4 (British Standard Institute, 1990b) 2.5 kg (light) compaction method.

3. Numerical model

A finite difference model was developed to capture the drying processes and eventual crack initiation and propagation using the ITASCA code, FLAC 2D v.4.00. FLAC was selected as it allows the user to access an in-built programming language FISH (Flac-ISH language), which enables complex geometry creation and variable dependent property functions to be automated. The model geometry (Fig. 1) represents the central cross-section through an indicative laboratory experiment consisting of a compacted soil mass within a steel, semi-circular mould (Fig. 2).

Bench top experiments were conducted in order to better constrain the model boundary conditions and for the purposes of numerical-physical model comparison. The steel moulds were approximately 10 times larger than moulds used for linear shrinkage testing according to BS 1377-2 (British Standard Institute, 1990a) while retaining the same length-width ratio.

A total of 5 experiments were conducted using material hand sieved to < 20 mm in order to remove coarse gravel and any substantial organic matter i.e. large roots. This was then air dried on a bench top before being wetted up to an initial water content of between 20 and 25% and allowed to equilibrate for a period of 48 h. The soil was then compacted in three layers using a 2.5 kg hammer to achieve a consistent dry density. This was based upon core cut samples of the in situ embankment fill which were found to have an average dry density of 1.65 Mg/m3, wet of optimum (15% optimum moisture content) at a depth < 1 m from the surface. Drying experiments subject to constant environmental conditions were run for a duration of 144 h (6 days). During this time, the specimen was systematically weighed at 0.5 h intervals for the first 5 h followed by daily intervals for the remaining time in order to ascertain the rate of water loss through drying for the given clay mass, density and drying configuration.

The upper mesh represents the remoulded clay component and comprises four-node quadrilateral elements, each equivalent to 3 mm^2. The soil-steel interface at the base of the experiment was simulated by incorporating a fully fixed region and horizontal interface elements that form a continuous plane subject to shear behaviour. Potential for crack generation was simulated by vertically orientated interfaces that allow the mesh to divide according to normal effective stress (e.g. Amarasiri et al., 2011; Sánchez et al., 2014). This facility is commonly used by numerical simulation packages to simulate jointing, faulting, bedding or any discontinuous feature of a material, typically in a rock mass (e.g. Helm et al., 2013). The general concept used to define the plane between two mesh regions is depicted in Fig. 3.

Grid-points positioned on both sides of the interface are recorded and checked for contact with their opposing neighbour. If for example, point N is found to lie on the segment between points M and P, then the vector normal to the interface is calculated. In addition to this, the length, L, is defined as half the distance to the nearest grid-point to the left (regardless of whether this grid-point is on the opposite or same

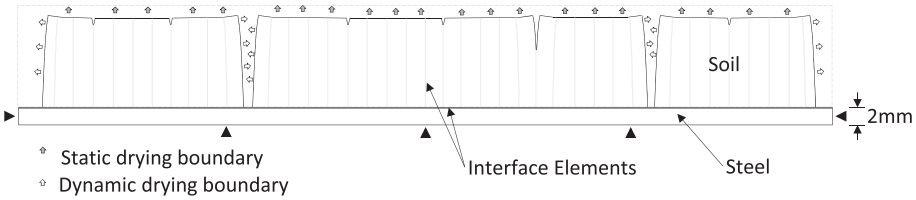

Fig. 1. Illustration of model geometry including interface elements and drying boundary condition locations [number of interface elements shown has been reduced for clarity].

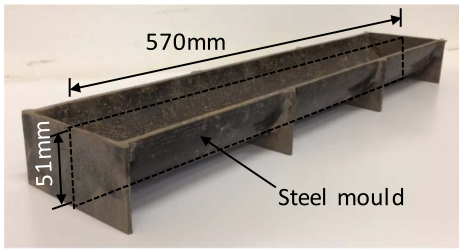

Fig. 2. Photograph showing indicative cracking experiment linear mould of semi-circular cross-section.

side) plus half that to the right. It is by this method that the interface is divided into connected segments. For each segment of the plane, the velocity of the associated grid-point is computed per time-step. Using the relation between velocity and displacement per time-step, the incremental displacement, and therefore force, is calculated and resolved into the normal and shear directions. The interface is able to accommodate slip according to the Coulomb shear-strength criterion:

$$F_{smax} = cL + \tan\phi F_n \quad (1)$$

where c = cohesion (Pa), L = effective contact length, ϕ = friction angle and Fn = effective normal force on the interface. The criterion for interface slip is satisfied if the shear force Fs = Fsmax. Crack interfaces are subject to a Rankine type tensile criterion – solely responsible for the bonded – un-bonded state of the interface elements. For further details regarding the interface formulation, see ITASCA, 2002.

It is recognised that this method prescribes possible crack locations and is therefore limiting in terms of crack spacing (6 mm) and orientation. However, indicative laboratory tests characterised the cracking trend as sub-vertical with a minimum spacing of approximately 15 mm and therefore, the interface spacing is suitable to capture the observed spacing of cracks under the simulated conditions.

The two-phase flow add-in to FLAC (ITASCA, 2002) was used to capture the fundamental, unsaturated processes during simulated drying. Through prescription of soil-water retention behaviour, negative pore pressure generation and relative permeability is made possible throughout the entire mesh and is not restricted to discontinuities.

3.1. Constitutive parameters

The increase in stiffness caused by drying-induced negative pore-water pressure was simulated by modifying the built-in FLAC elastic constitutive model using FISH to account for non-linearity. This was achieved by controlling Young's modulus as a function of soil-water content, ω and a constant, typical stiff clay Poisson's ratio of 0.3. The expression shown in Eq. 2 was constrained using experimental results from constant water content triaxial testing as described by Fredlund and Rahardjo (1993) and conducted on the study material by Mendes (2011).

$$E = 1770e^{-0.297\omega} \quad (2)$$

3.2. Basal interface properties

The basal interface properties were measured using an adapted direct shear apparatus by replacing the lower half with steel to simulate properties of the experiment mould. Testing was conducted at gravimetric water contents between 10 and 28% (the range of water contents measured in situ) with the resulting shear strength (kPa) and stiffness (kPa/m) trends as a function of water content input into the model

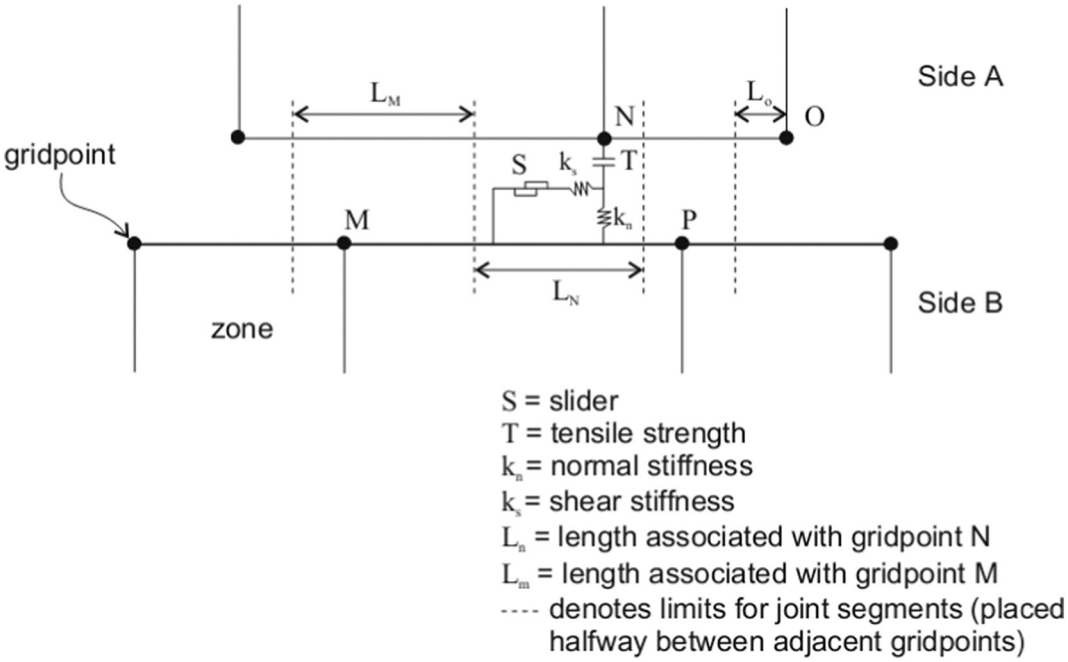

Fig. 3. Interface between sides A and B (after ITASCA, 2002).

(Stirling, 2014).

A friction angle of 35° ± 2.3° was determined at this contact and applied as a constant to the basal interface. At water content below 10–15%, the clay is assumed to be dislocated from the steel surface and able to undergo free sliding during shrinkage.

3.3. Crack interface properties

To capture crack formation, vertically orientated interface elements that pervade the mesh at a 2 element spacing (6 mm) were included (Fig. 1) and assigned a tensile bond failure criterion. Ultimate bond strength (σ_t) at each of the potential crack sites was defined as a function of water content (ω) according to Eq. 3. This relationship was established using a direct tensile apparatus (Stirling et al., 2015).

$$\sigma_t = 228.85e^{-0.14\omega} \quad (3)$$

Due to the developing vertical hydraulic gradient with drying, the depth along the interface at which saturation is taken and input to Eq. 2 will influence the strength value assigned to that interface. The crack tip is continually identified during the simulation on the basis of an interface threshold of 0.5 mm and this therefore allows the crack interface strength to be based on the tip saturation condition which controls ongoing crack propagation.

In order to better simulate a random distribution of crack initiation across the sample surface and associated localisation of crack strains, a degree of heterogeneity was introduced to the intact sample. Heterogeneity in the tensile strength distribution was incorporated through the use of a Gaussian distributed random number generator and a mean equivalent to the saturation dependent tensile strength for the given interface location. The specified standard deviation was based upon a sensitivity analysis conducted by Stirling (2014) whereby a SD of 2.5 was determined to best represent observed cracking patterns in the laboratory experiments.

A 26° angle of friction was measured by the standard direct shear test, BS1377-7 (British Standard Institute, 1990c). Within the model, friction angle is considered independent of saturation and remained constant, as was the case for the interpretation of unsaturated shear strength tests by Alonso et al. (1990).

3.4. Hydrological properties

Given the fundamental influence of water content on desiccation cracking, it is important to be able to model the unsaturated behaviour of the medium. To do this, the FLAC Two-Phase Flow add-in was employed (ITASCA, 2002). Darcy's law is used to define the wetting and non-wetting fluid flow according to their relative pressures. Full mechanical coupling is carried out using Bishop's effective stresses.

The van Genuchten approximation (van Genuchten, 1980) was employed to describe the capillary pressure (matric suction), P_c, and its fundamental link to the effective saturation using the following form:

$$S_e = \left[\left(\frac{P_c}{P_0}\right)^{\frac{1}{1-m}} + 1\right]^{-m} = \frac{S_w - S_r}{1 + S_r} \quad (4)$$

where the effective saturation, S_e, is related to the actual, S_w and residual saturation, S_r. The m parameter is a constant related to a further van Genuchten constant, n of the soil by $m = 1 - 1/n$ and is dependent on the pore-size distribution of the soil. The parameter corresponds to the soil air entry value (AEV) of suction. The van Genuchten fitting parameters and saturation variables were derived from the soil-water retention curve (SWRC) derived from laboratory testing of specimens of the Durham Boulder Clay, presented in Fig. 4 (Shehu, 2011). An air-entry value of 357 kPa and a van Genuchten n coefficient equal to 1.3 was established. A porosity equivalent to the saturated volumetric water content of 0.41 was prescribed. Furthermore, a FLAC saturated mobility coefficient of 1×10^{-12} m^2(Pa·s)$^{-1}$ was specified equating to a saturated hydraulic conductivity of 1×10^{-10} ms^{-1} as measured by field testing conducted on the as-placed material at a depth of < 0.5 m (Glendinning et al., 2014).

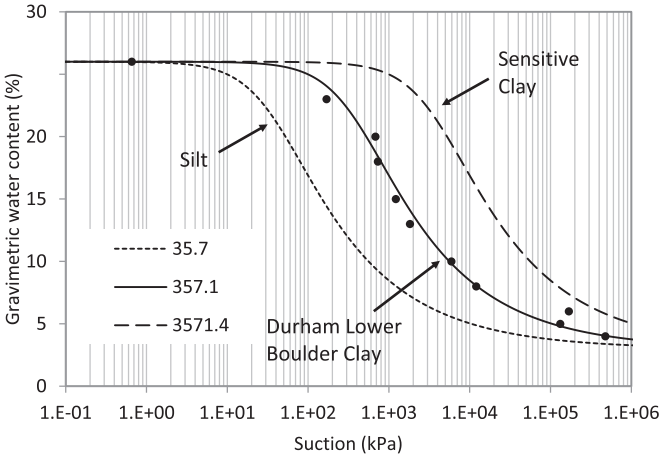

Fig. 4. SWRC determined by the filter paper technique.

3.5. Drying boundary condition

A dynamic discharge boundary condition was applied to simulate the drying flux. At the start of the model run, this boundary was located at the exposed upper surface of the clay mesh. As cracks develop, this boundary is extended to include the exposed end surfaces associated with shrinkage and the crack walls upon crack propagation as illustrated in Fig. 1.

The magnitude of the discharge associated with the extended boundary along the crack wall was 10% of the calculated initial, static discharge boundary. These surfaces are sheltered from atmospheric turbulence experienced at the upper surface leading them to be subject to a lower humidity gradient. Additionally, experimental evidence indicates that the crack wall possesses a hydraulic conductivity several orders of magnitude smaller than that of the matrix (Gerke and van Genuchten, 1993). This is assumed to suppress the evaporative loss from these surfaces.

A series of 3 laboratory experiments on specimens identical to those illustrated in Fig. 1 were subjected to varying drying conditions (2 repeats). The discharge rates were calculated where the evaporative surface area is assumed to be 5.81×10^{-2} m^2. An *initial* drying flux magnitude of 5.1×10^{-7} ms^{-1} corresponding to the start of Test 1 was selected for the purposes of model sensitivity analyses. This single rate is specified within the code and represents the maximum allowable discharge, though this will reduce with ongoing drying as the availability of water to the discharge boundary decreases.

4. Model behaviour

The ability of the model to capture realistic, comparable behaviour to that of the indicative laboratory experiments was evaluated where the simulated test 1 is herein considered as a baseline (representative) case. The model geometry following 6 days of applied drying (time to zero water content change) is presented in Fig. 5 which shows a total of 3 fully penetrating and 1 secondary, partially penetrating cracks along with 9 cracks of < 5 mm aperture.

The pattern of simulated cracks compares well with those observed in similar desiccation experiments. The asymmetry is a product of the imposed tensile strength heterogeneity with dislocation/shrinkage at the ends of the clay block in both cases inhibiting the generation of excessive surficial tensile stress. The first simulated crack initiation was recorded to occur at an equivalent water content immediately prior to air entry (i.e. still saturated), in agreement with experimental

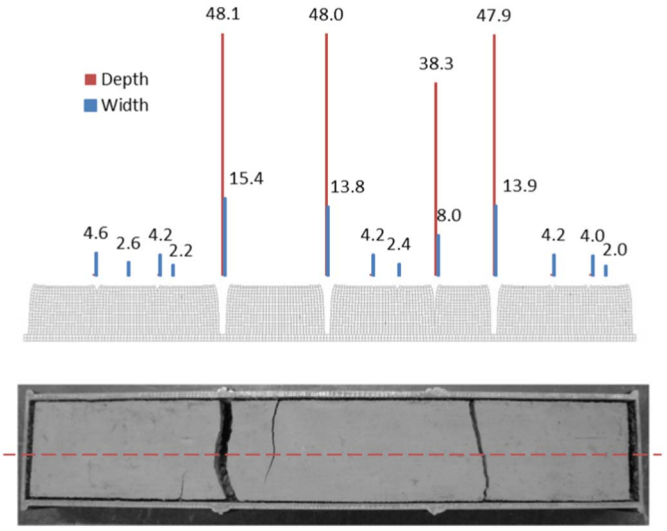

Fig. 5. Crack model response to baseline conditions including crack dimensions (mm) [Inset: photograph showing baseline test 5 at end of drying].

experience throughout the literature e.g. Rodriguez et al., 2007; Peron et al., 2009; Tang et al., 2010.

The formation of a concave, intact clay ped surface was also captured and is linked to the development of crack edge curling. This type of feature is common among polygonal desiccation features (Konrad and Ayad, 1997) and some linear laboratory experiments (Nahlawi and Kodikara, 2002). This specific phenomenon has been studied by other researchers; however, this is limited to scenarios of very thin soil layers (12.5-20 mm) (Hu et al., 2006; Kodikara and Choi, 2006).

The scale and style of modelled cracking appears to match observed behaviour well. However, surficial micro-cracks are less easily identified due to their small size and signify the breakup and weakening of the desiccated surface. Therefore, the onset and transient contribution to the total degree of cracking intensity of such features was quantified using the crack intensity factor (CIF) (Miller et al., 1998):

$$CIF = 100((\sum L_c + L_s)/L_o) \quad (5)$$

where, L_o is the original length of the clay layer after compaction, L_c and L_s represent the total crack apertures and total length minus end-shrinkage respectively. The development of CIF is presented in Fig. 6 and shows four stages of behaviour. The first stage shows total CIF to be entirely controlled by linear shrinkage (taken between the uppermost left- and right-hand grid-points) prior to crack initiation at hour 2. The second stage captures the initiation and development of primary cracking with linear shrinkage shown to reduce coincident with crack strain localisation (hours 2–3). During this stage, the contribution of crack development dominates the CIF trend. Stage three represents a

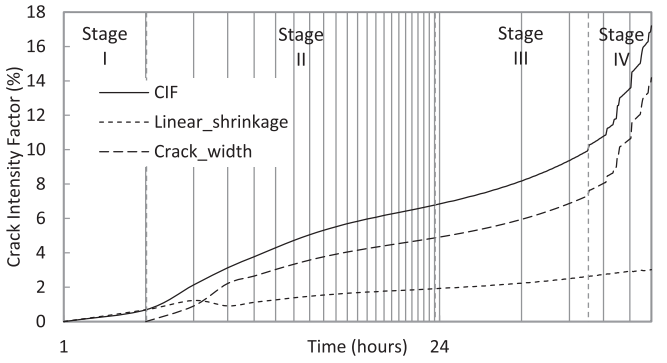

Fig. 6. Cracked model response and development of Crack Intensity Factor [logarithmic time axis used to aid presentation of early-stage behaviour].

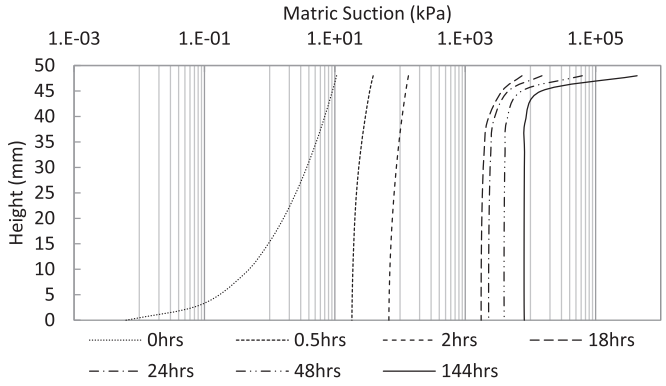

Fig. 7. Vertical suction profile at the middle of the mesh throughout simulated drying.

period of linear growth in established crack site widths and is accompanied by minor overall layer length shrinkage. Finally, stage four depicts very near-surface disintegration characterised by punctuated, shallow cracking events.

The development of the pore pressure profile within the clay layer is shown in Fig. 7 and indicates the mechanism behind the shallow disintegration in stage four. Note that the profile at '0 h' represents < 1 min following application of drying. Due to the logarithmic scale, it is not possible to present the hydrostatic profile at t_o = 0 h. However, it can be seen that a suction of 10 kPa at the drying, upper surface is rapidly generated while the base of the clay layer remains saturated. During the course of the first 2 h, the profile becomes approximately uniform with depth (reducing in range) while increasing in mean suction. Drying beyond 18 h is shown to produce little change in the magnitude of suctions over the majority of the layer depth. However, simulated suction values increase by up to 2 orders of magnitude at a progressively shallow depths. This signifies the development of a highly desiccated 'crust' which acts to hydraulically isolate the clay layer below it because it becomes increasingly difficult for water to be removed due to the reduced unsaturated permeability. Despite the specification of a maximum initial drying rate at the exposed boundary, the developing hydraulic profile is responsible for inhibiting total water removal.

4.1. Mechanical boundary sensitivity

To establish the influence of mechanical boundary conditions on simulated cracking, a series of sensitivity analyses were performed. The effect of basal boundary properties on crack development was tested by comparing the baseline model scenario with both fully fixed and free conditions. In the baseline scenario, the clay-mould interface is subject to measured shear conditions; however, a fixed boundary in the x-direction is equivalent to a vertically continuous case in which the thickness of the clay is infinite and lateral displacement is limited by the presence of further clay to depth. It is recognised that in the fixed case, zero displacement is an extreme of this scenario. The free case is highly idealised and may be considered only representative of specialised laboratory scenarios such as in the use of Teflon (Peron et al., 2009) or glass (Lecocq and Vandewalle, 2003; Vogel et al., 2005) mould constructions. As shown in Fig. 6, the free shrinkage scenario fails to generate sufficient tensile reactive stress and does not produce cracking, as experienced experimentally by Peron et al. (2009). The fixed base and empirical conditions are found to generate very similar cracking extents, potentially indicating that given the relative thickness of the modelled compacted fill layer, restrained shrinkage by a vertical continuum is captured. It is expected that basal influence will increase with decreasing clay layer thickness.

Modelling cracking in laboratory scale experiments inherently limits the lateral extent of the simulation necessitating the need for the mesh

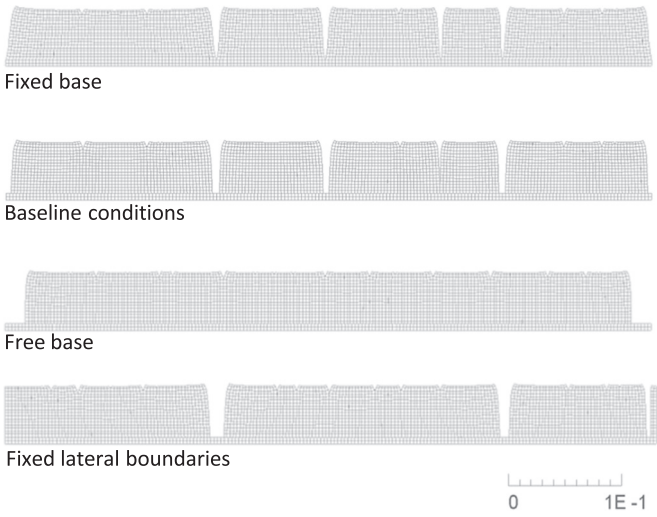

Fig. 8. Simulated cracking morphology under given mechanical fixities.

end boundaries to be kept free to account for linear shrinkage (as in the baseline case). However, in order to investigate cracking in a continuum, the baseline run was repeated with fixed lateral boundaries resulting in marginally fewer fully penetrating cracks than the free case (Fig. 8). The main difference is in the distribution of cracking across the mesh – the removal of any stress relief effect at the lateral boundaries results in crack distribution being solely governed by tensile strength heterogeneity.

4.2. Constitutive property sensitivity

The non-linear elastic constitutive law employed in this work describes the elastic modulus as a function of water content. This was designed to capture the increase in material stiffness with progressive drying. In order to investigate the influence of the elastic modulus function on cracking, the baseline, measured, relationship is compared to both a similar relationship reported in the literature and to a case representative of little to no gain in stiffness with reducing water content.

An expression for the change in modulus, H, with capillary pressure, P_c, was reported by Kodikara et al. (2004) after testing conducted on Werribee clay by Nahlawi (2004):

$$H = 24.0P_c^{0.95} \tag{6}$$

This was later recast by Kodikara and Choi (2006) using the SWRC into the form of Eq. 7 and by establishing that the clay remained saturated below the plastic limit. A Poisson's ratio of 0.45 was assumed and Eq. 8 was used to represent the change in Young's modulus with water content.

$$H = 3 \times 10^{10}\omega^{-4.070} \tag{7}$$

$$E = H(1 - 2v) \tag{8}$$

This function is presented in Fig. 9a in addition to the baseline, empirical trend and an artificially reduced version of the empirical relationship modified by reducing the intercept variable by 50% while maintaining the original exponent. This latter function was devised to test the scenario where little gain in stiffness is experienced upon drying and all other baseline conditions were maintained.

The resulting geometries from each simulation are presented in Fig. 9b in order of decreasing ultimate stiffness. It is evident that the more extreme stiffening trend of the highly reactive Werribee clay produced no initiation of cracking in this model and limited end-shrinkage. Tensile stresses generated by shrinkage due to simulated drying were insufficient to exceed the tensile strength of any single crack interface. However, cracking was initiated in the baseline case and it is observed that the same crack interfaces that fully penetrate the baseline mesh have also been exploited by drying in the reduced stiffening version of this case. For any given stage in the drying time, the lower elastic modulus results in greater shrinkage strain and ultimate crust disintegration as evidenced by the CIF history (Fig. 9c). By the end of stage three crack growth, the 50% reduced stiffening trend is shown to produce approximately double the crack intensity of the baseline conditions. Modelling cracking in this way has established the non-linearity of material stiffening with progressive drying to be the largest controlling factor on the initiation and subsequent growth of cracking.

4.3. Hydrological parameter sensitivity

4.3.1. Drying rate

In order to assess the sensitivity of the modelled cracking and desiccation crust response to fundamental hydraulic property ranges representative of exemplar soils, each property/condition was isolated and investigated. Within the model code, drying rate was imposed as a constant flux value although it is recognised that the flux experienced in the experiments is in proportion to the availability of water at the discharge boundary. A variety of rates were applied over a nominal 6 day period: three low rates from indicative laboratory results and two elevated rates. The model geometry responses are presented in Fig. 10a. It may be seen that lower rates produce well defined, fully penetrating cracks, while elevated drying rates produce a greater number of partially penetrating cracks. Crack propagation is related to the depth to which tensile stresses are developed with very high rates producing a restricting effect on the depth of tensile stress generation leading to extensive cracking only within the previously described crust. The CIF plot (Fig. 10b) demonstrates the positive effect increased drying rate has on near-surface deterioration and the reduced ultimate depth of the crust.

4.3.2. Hydraulic conductivity

It is widely accepted that deep cracking affects the bulk properties of an engineered fill by increasing infiltration of water to depth, causing a more rapid pore-water pressure response at depth, exacerbating pore pressure cycles and progressively softening clay-based soils. However, the matrix permeability of a given soil is shown to heavily influence the susceptibility of the material to the formation of cracks. The relative (unsaturated) hydraulic conductivity of the drying medium is a function of soil-water retention and is limited in the upper bound by the saturated hydraulic conductivity. The simulated crack morphology resulting from varied hydraulic conductivity about the baseline value is presented in Fig. 11.

The model demonstrates that materials of lower hydraulic conductivity are more susceptible to cracking (Fig. 11a). Soils possessing a conductivity $> 5 \times 10^{-10}\,\mathrm{ms}^{-1}$ show a similar overall CIF magnitude (Fig. 11b) with only the localisation of crack strain (crack spatial distribution) differing; however, the timing of greatest CIF increase (i.e. crack initiation) is delayed. Crack development is found to have occurred more rapidly in the lower conductivity simulations with stage four crust formation and disintegration only demonstrated by material of saturated hydraulic conductivity $< 1 \times 10^{-10}\,\mathrm{ms}^{-1}$ for the given soil/drying conditions. At hydraulic conductivity values lower than $1 \times 10^{-10}\,\mathrm{ms}^{-1}$, the reduced ability of water to migrate to the drying surface from depth under capillary forces accelerates the formation of the desiccated crust where the effects of drying (i.e. elevated suction and tensile stress generation) is most pronounced resulting in the maximum crack formation. This concept may be framed on the basis of common analogues for saturated hydraulic conductivity such as pore size distribution or clay mineral content. For example, extremely fine, clay rich soils are recognised to crack more readily than progressively coarser graded soils.

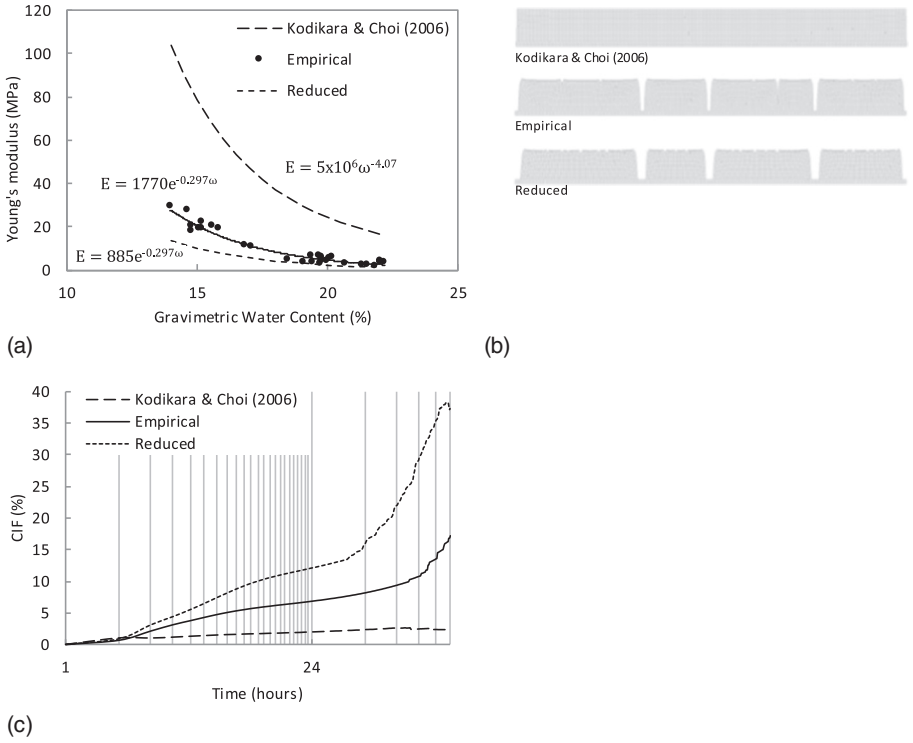

Fig. 9. Elastic function sensitivity (a) simulated elastic modulus trend variants (b) crack geometry and (c) CIF development.

4.3.3. Soil-water retention parameters

Further to saturated hydraulic conductivity is the water retention properties of fine grained soils and their influence upon the timing and typical morphology of cracking. The input van Genuchten SWRC fitting parameters, α and n, govern the generation of negative pore pressure with reducing water content by specifying the air entry value (AEV) and rate of de-saturation upon reaching this critical pressure, respectively.

The AEVs tested were varied from the glacial till baseline value by ± 1 order of magnitude, based on values of a silt, 20 kPa (Huang, 1994) and a sensitive clay, 2500 kPa (Fredlund, 1964) – these are shown in Fig. 4. The cracking response of the model (Fig. 12) was found to be very sensitive to the AEV where pervasive, fully penetrating cracking was captured in a high AEV simulation. This is the result of extremely high suctions being generated throughout the clay layer for a given moisture removal rate whilst a high unsaturated permeability was maintained. A reduced AEV was found to produce no penetrating, primary cracking and only shallow surface disintegration in the desiccated crust. This is depicted by the approximately constant rate of stage three CIF increase following initial end shrinkage.

The greatest model sensitivity was demonstrated by a change in the n coefficient. This meant that the tested range is relatively narrow in comparison to the reference materials given above. This was due to numerical instability related to the rapid change in effective stress dependent variables (including elastic moduli) in a given time-step. The values tested are presented in Fig. 12 alongside the baseline value of 1.3.

A trend towards less fully penetrating cracking is produced through the use of a higher n, steeper SWRC. However, this is manifested as only a 1% lower CIF at the end of stage three. The most striking difference is the onset of stage four, surface deterioration. Progressively greater crust deterioration is evident upon using a lower n, less steep SWRC. In the greater drying scenario produced by the use of a high n coefficient, water removal is more evenly distributed through the clay profile. On the other hand, although a lower overall water removal was observed using a low n, for any given water content, a higher magnitude of suction is calculated. Therefore, higher surface tensile stresses are observed to result from the implementation of a shallow, more slowly desaturating SWRC following air entry.

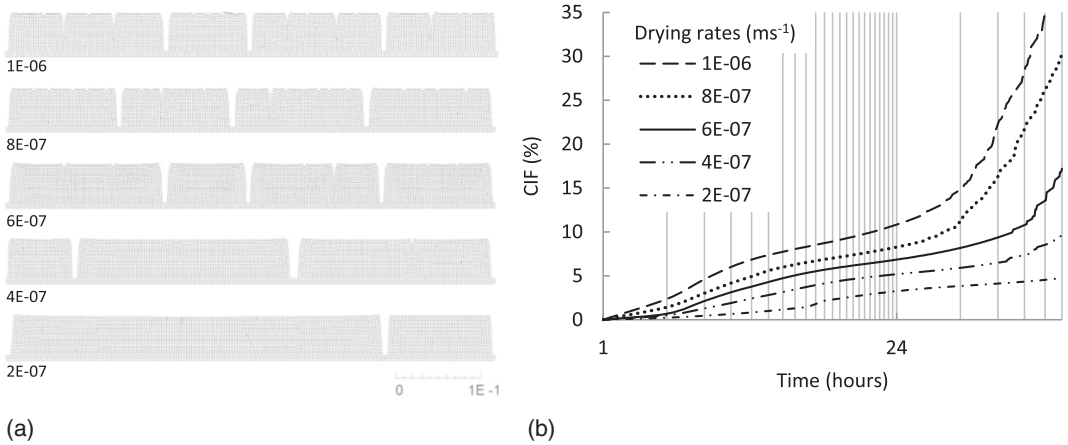

Fig. 10. Simulated cracking under varied drying rates (ms^{-1}) (a) crack geometry and (b) CIF development.

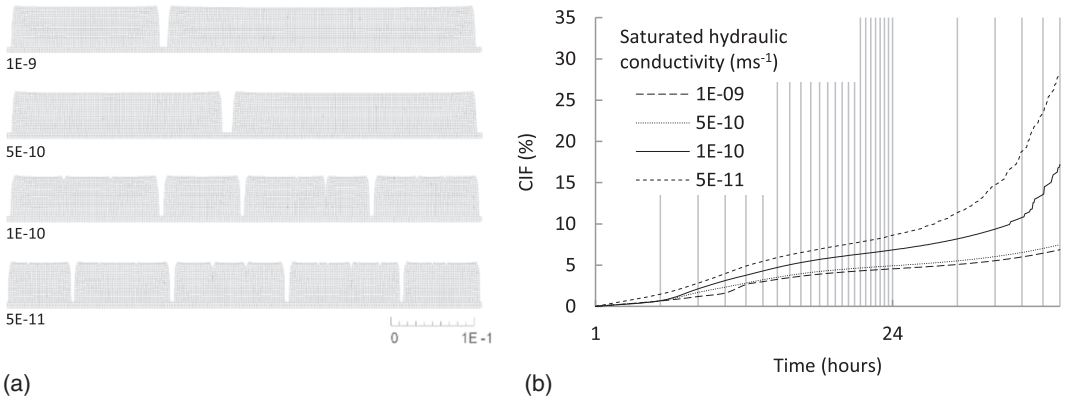

Fig. 11. Simulated cracking under varied saturated hydraulic conductivity values (ms^{-1}) (a) crack geometry and (b) CIF development.

4.4. Sensitivity to tensile strength development

Further to establishing the laboratory trend of increased tensile strength along the primary drying curve used in the baseline conditions (Stirling et al., 2015), a testing program was conducted to investigate the tensile strength change with cyclic drying and wetting as reported by Stirling et al. (2014). The data presented in Fig. 13a shows this relationship along an initial drying, wetting and subsequent re-drying path.

The initial drying path shows a typical trend of exponentially increasing tensile strength with decreasing water content. Upon re-wetting, a similarly exponential trend may be approximated. However, the wetting relationship follows much lower strength values and at water contents > 20%, negligible tensile stress is maintained. The second drying path exhibits higher tensile strengths than that of the wetting trend yet is considerably weaker than the initial drying curve.

The relationship is shown to undergo translation towards the origin upon cyclic wetting and drying. Hysteretic phenomena are familiar in the context of soil-water retention – where upon wetting, lower suction is developed at a given water content than would be generated upon drying. This effect may well contribute to the reduced strength shown along the wetting path. However, strength reduction may well also be attributable to the micro-scale cracking during the initial desiccation stage causing an increment of non-recoverable deterioration in the structure of the compacted clay fabric.

Crack initiation is assumed to occur when the induced tensile stress exceeds the soil tensile strength. A cracking analysis on this basis alone would indicate that crack initiation occurs at a given tensile strength which exists at a specific water content. Should the cracking condition have been met under initial drying then sufficient stress 'relaxation' may well take place whereby subsequent generation of tensile stress does not exceed the critical tensile strength and no further cracking takes place. Hence, the use of a single, initial drying relationship results in an underestimation of crack network development. By establishing lower tensile strengths as a result of wetting-drying cycles, the criterion by which crack initiation occurs is met by the generation of yet lower tensile stresses. This leads to progressively increased cracking with cycling. The authors anticipate that a residual tensile strength will be reached after a number of repeated drying and wetting cycles and no further strength reduction occurs. The deterioration in tensile strength to residual conditions is further evidenced by the marked reduction in water content at cracking after an average of three drying cycles, as reported by experimenters working on both clay slurries (Tang et al., 2008; Tang et al., 2011) and compacted clays (Yesiller et al., 2000).

In order to explore the effect of reduced tensile strength on cracking, the exponential relationship input to the model was modified. The chosen trend variations are presented in Fig. 13b where it may be seen that at any given point upon the measured trend line, the tested values represent ± a given percentage value. This approach is believed to capture a more realistic development of tensile strength from a relatively low magnitude at high water contents. As presented by Stirling et al. (2015), the greatest repeatability and minimum deviation from the regression line was towards the wetter extent of the data, it is therefore justifiable that this end is subject to the least variation.

The simulated crack geometries may be seen to have been affected relatively little by a − 10% change in the tensile strength, though a + 10% change produces one less full crack (Fig. 13c). This trend is as expected with larger tensile stresses required to initiate cracking in higher tensile strength simulation. However, the simulation at + 20% has reverted to three fully and one partially penetrating cracks, similar to that of the 0 and − 10%. However, the position of these cracks is observed to have been altered with cracks appearing towards the more

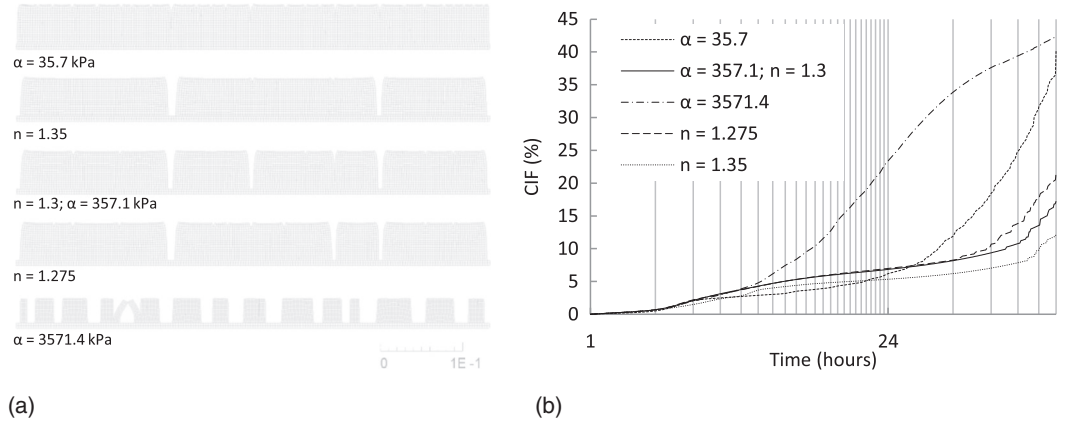

Fig. 12. Simulated cracking under varied SWRC AEV (α) and *n* coefficients (a) crack geometry and (b) CIF development.

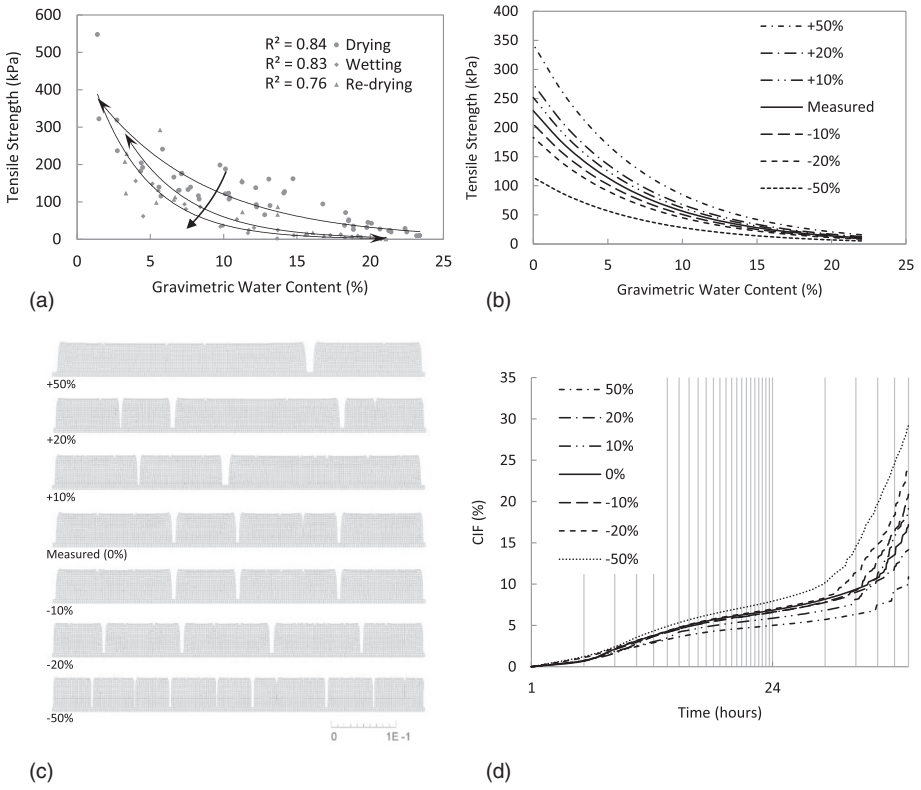

Fig. 13. Tensile strength magnitude sensitivity (a) measured reduction in tensile strength upon hydric cycling (b) simulated tensile strength function variants (c) crack geometry and (d) CIF development.

freely shrinking boundaries. In line with the requirement for a lower tensile stress to initiate cracking in the lower tensile strength cases, four fully penetrating cracks are evident when a − 20% magnitude is applied. Very different cracking morphologies are apparent in the ± 50% simulations with many more narrow and partially penetrating cracks in the lower tensile strength test than in the coherent, clod-like behaviour of the strongest simulation. This is also reflected in the steadily diverging CIF data across the range of applied strength trends (Fig. 13d). In addition to the greater overall crack intensity exhibited by the weaker strength trends, earlier onset of surface disintegration is shown and is a consequence of lower surficial stresses required to break the interface bonds. The outlier to the order of systematically more rapid CIF gain with reducing strength simulations between the extremes of ± 50% is the CIF for + 10%. With only two fully penetrating cracks, stages one and two show CIF development below that of + 20% as well as unexpectedly large surface deterioration. It is not fully understood why this has occurred although with such a minor variation from the baseline case, it is proposed that numerical rounding in the solution scheme may be responsible.

The tensile strength magnitude employed has been found to influence the cracking style of the model output with a trend towards higher strength producing fewer, wider cracks with little surface disintegration. Conversely, a trend towards lower strength has been found to produce a larger number of narrow, closely spaced cracks with a large component of crust disintegration. In the context of wetting-drying cycles therefore, the successive shift from higher to lower strength in the model is shown to heavily influence the development of crack prevalence and style from an individually coherent clod assembly to a finer, more aggregated structure.

5. Conclusions

The results of this study have demonstrated the ability of the model to capture the principle desiccation and cracking mechanism. Drying induced negative pore pressures generate tensile stress due to the developing hydraulic gradient throughout the soil profile, this then exceeds the tensile strength of the soil resulting in crack initiation. With ongoing drying, the balance between material stiffness and strength increase, and the generation of elevated suctions and associated tensile stress, leads to strain localisation (i.e. propagation of existing cracks). Prolonged drying is shown to result in the formation of a desiccated crust typically on the order of < 10 mm depth and is characterised by highly negative pore pressures and extremely low relative permeability. This feature acts to hydraulically isolate the wetter layer immediately beneath, slowing drying and potentially inhibiting infiltration. In the environment, this is likely to lead to an increase in run-off during high intensity summer rainfall events. Since run-off is understood to be intercepted by cracked in-situ soil, it is inferred from the crust formation modelled that accelerated by-pass flow to depth could be facilitated and that the critical suctions necessary to the stability of many geotechnical assets could be dissipated.

The deterioration processes presented are understood to be dependent upon the combined influence of material properties and external drivers such as drying rate and duration in addition to the action of wetting-drying cycles. The severity with which this deterioration mechanism acts is dependent on the construction material, largely determined by local geology and as such will vary geographically. Based on the model sensitivity analysis, the most sensitive materials are those that exhibit high AEV and extremely low permeability typical of high plasticity materials such as marine derived soils. Examples of these materials are, for example, commonly found in the south east of the UK (e.g. London Clay, Gault Clay, Weald Clay). The results of the research presented herein show that these materials are likely to exhibit pervasive, fine cracking patterns, while the intermediate plasticity, well graded glacial tills (such as those present in the northern UK) are likely to exhibit permanent, deep cracking but less desiccated crust development.

Tensile strength reduction caused by wetting-drying cycles (established by laboratory testing) provide evidence for the implications of seasonal cycles on the deterioration of the near-surface of geotechnical soil structures, such as transportation and flood protection embankments. In addition to the influence of hysteretic phenomena,

cumulative micro-cracking is shown to reduce the ability of the soil to resist drying induced tensile stresses and contributes to the progressive disaggregation of the soil surface.

The drying rate is shown to influence not only the timing of both the initiation and following propagation of significant cracking, but also the final cracking extent prior to crust formation. Elevated drying rate scenarios are shown to exhibit more numerous primary cracks and a greater degree of surface disintegration behaviour. Therefore, the deterioration process of desiccation cracking is set to accelerate with anticipated higher temperatures.

The sensitivity analyses presented demonstrate the capability of the model to handle parameter ranges that cover a very wide range of clay mineral rich soil types including sensitive, shrink/swelling clays. Whilst the influence of model parameters have been assessed in isolation, the combination of parameter variations from the baseline material case presented is wholly feasible. However, to best capture the behaviour of a specific soil, it is recommended that the SWRC, stiffness and tensile strength be determined. It is important to note that the model is particularly sensitive to the SWRC parameter 'n' – related to the pore size distribution. The range in 'n' over which the model remains numerically stable is comparatively narrow and represents the main limitation to the robustness of the model.

The work presented in this paper has demonstrated that an understanding of deterioration processes, such as the progressive loss of material strength with seasonal cycling, is crucial to the understanding of the complexities of soil-atmosphere interaction and provides a scientific underpinning for the relationship of geotechnical infrastructure with our changing climate. The results point towards a future acceleration of deterioration, and the potential demand for significantly higher investment in infrastructure maintenance.

Acknowledgements

The authors would like to acknowledge the collaborative research projects iSMART (Grant number EP/K027050/1) and ATU (Grant number EP/K021699/1) funded by the UK Engineering and Physical Sciences Research Council (EPSRC).

References

Albrecht, B.A., Benson, C.H., 2001. Effect of desiccation on compacted natural clay. J. Geotech. Geoenviron. Eng. 127, 67–75.
Alonso, E.E., Gens, A., Josa, A., 1990. A constitutive model for partially saturated soils. Geotechnique 40 (3), 405–430.
Amarasiri, A.L., Kodikara, J.K., Costa, S., 2011. Numerical modelling of desiccation cracking. Int. J. Numer. Anal. Methods Geomech. 35, 82–96.
British Standard Institute, 1990a. BS 1377-2: Methods of Test for Soils of Civil Engineering Purposes Part 2: Classification Tests. BSI, Milton Keynes UK.
British Standard Institute, 1990b. BS 1377-4: Methods of Test for Soils of Civil Engineering Purposes Part 4: Compaction-related Tests. BSI, Milton Keynes UK.
British Standard Institute, 1990c. BS 1377-7: Methods of Test for Soils of Civil Engineering Purposes Part 7: Shear Strength Tests (Total Stress). BSI, Milton Keynes UK.
Fredlund, D.G., 1964. Comparison of Soil Suction and One-dimensional Consolidation Characteristics of a Highly Plastic Clay. MSc thesis University of Alberta, Canada.
Fredlund, D.G., Rahardjo, H., 1993. Soil Mechanics for Unsaturated Soils. Wiley, New York.
Gerke, H.H., van Genuchten, M.T., 1993. Evaluation of a first-order water transfer term for variably saturated dual-porosity flow models. Water Resour. Res. 29 (4), 1225–1238.
Glendinning, S., Hughes, P.N., Helm, P., Chambers, J., Mendes, J., Gunn, D., Wilkinson, P., Uhlemann, S., 2014. Construction, management and maintenance of embankments used for road and rail infrastructure: implications of weather induced pore water pressures. Acta Geotech. 9 (5), 799–816.
Helm, P.R., Davie, C.T., Glendinning, S., 2013. Numerical modelling of shallow abandoned mine working subsidence affecting transport infrastructure. Eng. Geol. 154, 6–19.
Huang, S.-Y., 1994. Evalution and Laboratory Measurement of the Coefficient of Permeability in Deformable, Unsaturated Soils. PhD thesis University of Saskatchewan, Canada.
Hughes, P.N., Glendinning, S., Mendes, J., Parkin, G., Toll, D.G., Gallipoli, D., Miller, P., 2009. Full-scale testing to assess climate effects on embankments. Eng. Sustain. 162 (2), 67–79.
Hulme, M., Jenkins, G.J., Lu, X., Turnpenny, J.R., Mitchell, T.D., Jones, R.G., Lowe, J., Murphy, J.M., Hassell, D., Boorman, P., McDonald, R., Hill, S., 2002. Climate Change Scenarios for the United Kingdom: The UKCIP02 Scientific Report. Tyndall Centre for Climate Change Research, School of Environmental Sciences, University of East Anglia, Norwich, UK.
Hu, L., Peron, H., Hueckel, T., Laloui, L., 2006. Numerical and phenomenological study of desiccation of soil. Advances in unsaturated soil, seepage and environmental geotechnics. ASCE Geotech. Spec. Publ. 192 (17), 166–173.
ITASCA, 2002. FLAC User's Guide. ITASCA, Minnesota, USA.
Jenkins, G., Murphy, J., Sexton, D., Lowe, J., Jones, P., Kilsby, C., 2010. UK Climate Predictions Briefing Report. UK Climates Impacts Programme.
Jones, L.D., Jefferson, I., 2012. Expansive soils. In: Burland, J., Chapman, T., Skinner, H., Brown, M. (Eds.), ICE Manual of Geotechnical Engineering. Volume I: Geotechnical Engineering Principles, Problematic Soils and Site Investigation ICE Publishing, London, pp. 413–441.
Kodikara, J.K., Choi, X., 2006. A simplified analytical model for desiccation cracking of clay layers in laboratory tests. ASCE Geotech. Spec. Publ. 2, 2558–2569.
Kodikara, J.K., Nahlawi, H., Bouazza, A., 2004. Modelling of curling in desiccating clay. Can. Geotech. J. 41 (3), 560–566.
Konrad, J.-M., Ayad, R., 1997. An idealized framework for the analysis of cohesive soils undergoing desiccation. Can. Geotech. J. 34, 477–488.
Lecocq, N., Vandewalle, N., 2003. Dynamics of crack opening in a one-dimensional desiccation experiment. Physics A 321 (3–4), 431–441.
Mendes, J., 2011. Assessment of the Impact of Climate Change on an Instrumented Embankment – An Unsaturated Soil Mechanics Approach. PhD Thesis School of Engineering and Computer Sciences, Durham University, UK.
Miller, C.J., Mi, H., Yesiller, N., 1998. Experimental analysis of desiccation crack propagation in clay liners. J. Am. Water Resour. Assoc. 34 (3), 677–686.
Nahlawi, H., 2004. Behaviour of a Reactive Soil during Desiccation. MEng thesis Department of Civil Engineering, Monash University, Australia.
Nahlawi, H., Kodikara, J., 2002. Experimental observations on curling of desiccating clay. In: Jucá, J.F.T., de Campos, T.M.P., Marinho, F.A.M. (Eds.), Unsaturated Soils: Proceedings of the Third International Conference on Unsaturated Soils, UNSAT 2002 Volume 2. CRC Press, London, pp. 553–556.
Nahlawi, H., Kodikara, J.K., 2006. Laboratory experiments on desiccation cracking of thin soil layers. Geotech. Geol. Eng. 24, 1641–1664.
Peron, H., Hueckel, L., Laloui, L., LB, Hu, 2009. Fundamentals of desiccation cracking of fine-grained soils: experimental characterisation and mechanisms identification. Can. Geotech. J. 46 (10), 1177–1201.
Rodriguez, R., Sanchez, M., Ledesma, A., Lloret, A., 2007. Experimental and numerical analysis of desiccation of a mining waste. Can. Geotech. J. 44, 644–658.
Sánchez, M., Manzoli, O.L., Guimarães, L.J.N., 2014. Modelling 3-D desiccation soil crack networks using a mesh fragmentation technique. Comput. Geotech. 62, 27–39.
Shehu, A.A., 2011. Determination of the Wetting Portion of the Soil Water Retention Curve for the BIONICS Embankment Soil Using the Filter Paper Technique. MSc thesis School of Civil Engineering and Geosciences, Newcastle University, UK.
Stirling, R.A., 2014. Multiphase Modelling of Desiccation Cracking in Compacted Soils. PhD Thesis School of Civil Engineering and Geosciences, Newcastle University, UK.
Stirling, R.A., Hughes, P.N., Davie, C.T., Glendinning, S., 2014. Cyclic relationship between saturation and tensile strength in the near-surface zone of infrastructure embankments. In: Khalili, K., Russell, A., Koshghalb, A. (Eds.), Unsaturated Soils: Research and Applications. CRC Press, London, pp. 1501–1505.
Stirling, R.A., Hughes, P., Davie, C.T., Glendinning, S., 2015. Tensile behaviour of unsaturated compacted clay soils — a direct assessment method. Appl. Clay Sci. 112–113, 123–133.
Tang, C.-S., Cui, Y.-J., Shi, B., Tang, A.-M., Liu, C., 2011. Desiccation and cracking behaviour of clay layer from slurry state under wetting–drying cycles. Geoderma 166, 111–118.
Tang, C.-S., Cui, Y.-J., Tang, A.-M., Shi, B., 2010. Experiment evidence on the temperature dependence of desiccation cracking behaviour of clayey soils. Eng. Geol. 114, 261–266.
Tang, C.-S., Shi, B., Liu, C., Zhao, L., Wang, B., 2008. Influencing factors of geometrical structure of surface shrinkage cracks in clayey soils. Eng. Geol. 101, 204–217.
Tran, D.T.Q., Fredlund, D.G., Chan, D.H., 2016. Improvements to the calculation of actual evaporation from bare soil surfaces. Can. Geotech. J. 53, 118–133.
van Genuchten, M.T., 1980. A closed-form equation for predicting the hydraulic conductivity of unsaturated soils. J. Soil Soc. Am. 44 (5), 892–898.
Vogel, H.-J., Hoffmann, H., Roth, K., 2005. Studies of crack dynamics in clay soil 1. Experimental methods, results and morphological quantification. Geoderma 125, 203–211.
Wilson, G.W., Fredlund, D.G., Barbour, S.L., 1997. The effect of soil suction on evaporation fluxes from soil surfaces. Can. Geotech. J. 34 (4), 145–155.
Yesiller, N., Miller, C.J., Inci, G., Yaldo, K., 2000. Desiccation and cracking behavior of three compacted landfill liner soils. Eng. Geol. 57, 105–121.